



Research Article

A DFT study to determine the structure and composition of ϵ - W_2B_{5-x} S.S. Setayandeh^{a,*}, E.G. Obbard^a, J. Stansby^a, D. Frost^a, Jack O. Astbury^b, C.L. Wilson^b, P.A. Burr^a^a School of Mechanical and Manufacturing Engineering, University of New South Wales, Kensington 2052, NSW, Australia^b Tokamak Energy Ltd, 173 Brook Drive, Milton Park, Oxon OX14 4 SD, United Kingdom

ARTICLE INFO

Article history:

Received 1 February 2022

Received in revised form 4 April 2022

Accepted 8 April 2022

Available online 12 April 2022

Keywords:

Tungsten boride

Ab initio calculations

Neutron diffraction

X-ray diffraction

ABSTRACT

There is no consensus in the literature on the structure and composition of the ϵ phase of the W-B system, variously reported as WB_2 and W_2B_5 . We used ab initio calculations at two levels of theory to identify the stable crystal structure and stoichiometry of this phase. Among the sixteen structures investigated in the composition range of 67–71.4 at% B (WB_2 – W_2B_5), nine exhibited unfeasibly high formation energies; the remaining seven were dynamically stable (did not exhibit any soft phonon modes), and satisfied mechanical stability criteria. When including the thermal vibrational contribution to the free energy, all structures with the W_2B_5 composition lay above the convex hull, suggesting that this composition is metastable, while those with WB_2 composition lay on the convex hull or within DFT precision of the convex hull. We found that four of the candidate structures exhibit negative vacancy formation energy, suggesting that the structures are unstable, or that they are naturally hypo-stoichiometric. Combining these results with a comparison of simulated and experimental x-ray and neutron diffraction patterns, we concluded that the ϵ phase is most likely a hypo-stoichiometric W_2B_{5-x} compound with space group $P6_3/mmc$.

© 2022 Published by Elsevier B.V.

1. Introduction

Tungsten borides are a class of ultra-hard high temperature ceramics (Vickers hardness \approx 42 GPa for tungsten tetraboride [1]), with outstanding physical and chemical properties, including chemical inertness, thermal shock and high-temperature electrical resistance [2–4] that compete with those of traditional hard materials [5–12]. The rich array of physical behaviours of tungsten borides has made them strong candidates for refractory and high temperature applications [13–18]; and recently they have been highlighted as promising candidate materials for radiation shielding of nuclear fusion applications [19,20]. In particular, the spherical tokamak reactor design [21] has limited space between the high energy fusion plasma and the cryogenically-cooled superconducting magnets, and therefore require materials with exceptional shielding performance, offered by tungsten borides [22].

The first complete report of phase diagram of the tungsten-boron system can be traced back to 1963 by Kieffer et al. [23]. Since then, five phases have been identified for the W-B system: W_2B (γ phase) [24,25], WB (variously reported as α or β phase) [24,26], WB_2 ($A1B_2$ -type structure) [27], W_2B_5 (ϵ phase) [24,28] and WB_4 [29]. The γ , α (β)

and ϵ phases occur at compositions of about 33.3, 50 and 70 at%B, respectively [24]. Determination of crystal structures of these compounds, especially boron-rich compounds ($B > 50\%$), has been challenging and in some cases it remains unclear [30]. This is partly because atomic scattering factor of x-rays scales with Z^2 , so structure factors are dominated by W ($Z = 74$), with low sensitivity to occupancy or position of B ($Z = 5$). Neutron scattering, on the other hand, is challenging due to the high cross-section for neutron absorption of B-10.

For the ϵ phase in particular, not only is the structure uncertain [8], but the composition has also been reported across a range spanning 65–71.4 at% B, such as W_2B_5 [24], WB_2 (W_2B_4) [8,31], $WB_{2.27}$ [32], W_2B_{5-x} [26] and W_2B_{4-x} [33]. The first report of the ϵ phase was by Kiessling in 1947 [24], who reported a composition of W_2B_5 (71.4 at% B) and a hexagonal crystal structure with space group $P6_3/mmc$, obtained from single crystal X-ray diffraction. The proposed structure comprises two types of boron layers: a graphite-like planar layer and a six-membered zig-zag layer with one boron atom located in the centre (see Fig. 1a). Later work by Frotscher et al. in 2007 [8] indicated that the ϵ phase is better described by a W_2B_4 composition (66.7 at% B), in which the boron atom site in the center of the six-membered zig-zag layer is removed (Fig. 1b). However, the experimental results from neutron diffraction remained inconclusive [8]. Kayhan et al. in 2013 [33], proposed a new composition, W_2B_{4-x} ,

* Corresponding author.

E-mail address: s.setayandeh@unsw.edu.au (S.S. Setayandeh).

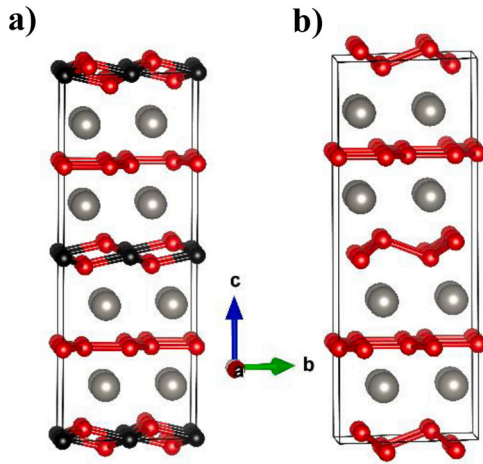


Fig. 1. Unit cells of a) W_2B_5 structure suggested by Kiessling [24], and b) W_2B_4 reported by Frotscher et al. [8], both with space group $P6_3/mmc$. Large grey atoms are W and small red atoms are B. Small black atoms in panel a are B atoms located in the centre of the six-membered zig-zag layers.

with space group $P6_3/mcm$ based on the neutron diffraction, in which a further boron atom was partially removed (occupancy of 0.166) in the graphite-like layers. However, this proposed composition (62 at% B) deviates significantly from the density measurements reported by Kiessling (71.4 at% B). The proposed structure was largely based on relative intensity of the neutron diffraction peaks [33], and therefore would be strongly sensitive to sample texture, perhaps explaining part of the disagreement.

Overall, the exact composition and atomic coordinates of the ϵ phase remain unclear. Modern computational structure searching tools such as USPEX [34–36], CALYPSO [30], and AIRSS [37] are a powerful way to explore the relative stability of a vast number of candidate structures. Employing these methods, recent studies by Li et al. [30] and Cheng et al. [38] suggested several structures that might be promising candidates for W_2B_5 . Due to the large number of potential candidates to screen, these studies base their results only on the ground state formation energy, of perfect (undefective) and stoichiometric crystals. They do not consider the full thermodynamics of phase stability, nor their dynamical or mechanical stability, or the potential deviation from stoichiometry. To date, there has been no in-depth study on the stability of these and other potential candidate structures that can provide conclusive information on the structure and composition of ϵ tungsten boride.

Due to the technological importance of boron-rich tungsten borides, and specifically for neutron shielding applications where the performance is strongly sensitive to the boron atomic density, it is a pressing task to resolve this question unambiguously. For this purpose, we revisit the available literature and re-interpret the experimental observations in light of new computationally-derived results. Here, we use ab-initio calculations to identify the crystal structure and stoichiometry of the ϵ phase in the W-B system. We assess phase stability based on thermodynamics, lattice dynamic, mechanics and point defect chemistry, in the temperature range 0–2500 K. For the most promising candidates, we report the calculated x-ray and neutron diffraction patterns and elastic constants to aid further experimental studies.

2. Methodology

All DFT simulations were carried out using the Vienna Ab-Initio Simulation Package (VASP) [39–41], using two exchange correlation functionals: the local density approximation (LDA) [42] and the Perdew, Burke, and Ernzerhof (PBE) formulation of the generalised gradient approximation [43]. Where only one set of results is

reported, it is for the PBE functional unless stated otherwise. Atoms were described with PAW pseudo-potentials [44,45] from the VASP 5.3 repository with three and six valence electrons for B and W respectively and a consistent plane-wave cut-off of 400 eV. The Monkhorst-Pack method [46] was applied to sample the electronic wave functions in Brillouin zone on a k point grid with a density of 31.4 \AA^{-3} in all directions, which produced results converged to $\pm 10^{-2}$ eV compared to a highly dense grid (47 \AA^{-3}). Partial occupancies were treated with a first-order Methfessel-Paxton smearing function of width 0.1 eV [47]. All structures were optimised by relaxing their lattice parameters and internal atomic coordinates. The formation enthalpy per atom, E_f , was calculated as:

$$\Delta E_f = \frac{\mu(W_xB_y) - x\mu(W) - y\mu(B)}{x + y} \quad (1)$$

where μ is the chemical potentials of the compound and reference phases. In the first instance this is taken to be the DFT total energy of a unit cell containing x W and y B atoms for the boride, and half the DFT energy of a tungsten bcc unit cell and one thirty-sixth of the DFT energy of an α -B unit cell for $\mu(W)$ and $\mu(B)$, respectively. For a more complete description of the formation energy, we also consider the vibrational energy and vibrational entropy contributions ($\Delta F^{vib} = \Delta E^{vib} + T\Delta S^{vib}$) to the stability of the boride. Thus, the formation free energy per atom, F_f , was similarly calculated as:

$$\Delta F_f = \Delta E_f + \Delta F^{vib} \quad (2)$$

where F^{vib} is calculated from the phonon frequencies (ω_i) at temperature T within the harmonic approximation, via a supercell approach, as [48]:

$$F^{vib} = \frac{1}{2} \sum_i^{3N} \hbar\omega_i + k_B T \sum_i^{3N} \ln \left(1 - e^{-\frac{\hbar\omega_i}{k_B T}} \right) \quad (3)$$

where k_B and N stand for the Boltzmann constant and number of atoms, respectively. The dynamical matrices for the phonon calculations [49] were computed using the Phonopy package [50].

Elastic constants were obtained by applying displacements of $\pm 0.01 \text{ \AA}$ and $\pm 0.02 \text{ \AA}$ in each symmetrically independent direction of the crystal. The elastic constants were fitted to the response of energy and atomic forces to the applied displacements, following the algorithm built into VASP [39–41]. The effect of ionic relaxation on elastic constants was also taken into account, although it was never greater than 4.7% of the primary stiffness constants. Bulk and Shear moduli were obtained assuming a polycrystalline aggregate, as described in the Hill method [51] of averaging Voigt [52] and Reuss [53] bounding cases.

Formation enthalpy of dilute point defect was calculated as:

$$E_{Defect} = E_{tot}(Defect) - E_{tot}(Perfect) - \sum n_i \mu_i \quad (4)$$

where $E_{tot}(Defect)$ and $E_{tot}(Perfect)$ are the total energy of the supercell with one defect and its equivalent perfect supercell, respectively. n_i and μ_i denote the number of atoms i removed from ($-n_i$) or added to ($+n_i$) the supercell to form the defect, and their corresponding chemical potential, respectively. The XRD and neutron data simulations were carried out by application of GSAS-II software [54].

3. Results and discussion

3.1. Thermodynamic stability

Twenty-three reported polymorphs of tungsten boride (W_xB_y), in the composition range of 50–80 at% B, were investigated. The stability of all structures was quantified via calculation of formation enthalpy per atom (Eq. 1) at ground state, with the PBE exchange-correlation functional. These are presented in Fig. 2 in the form of a convex hull. In principle, the convex hull connects the lowest

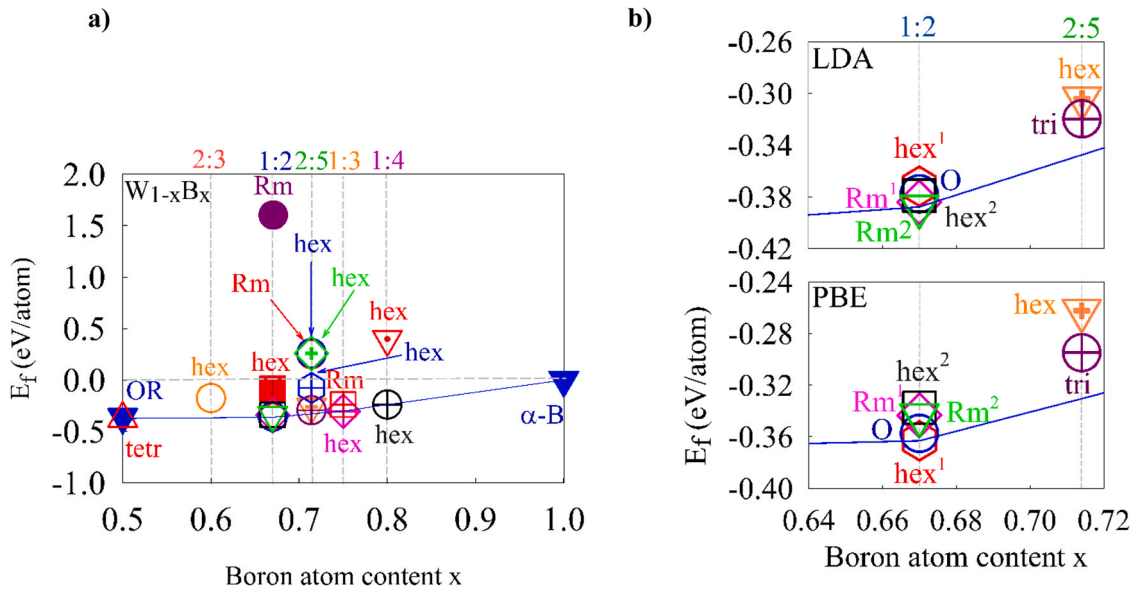


Fig. 2. a) Convex hull diagram for the B-rich side of the W-B system, obtained with the PBE exchange correlation functionals. Panel b) illustrates the region of the ϵ phase obtained with the PBE and LDA.

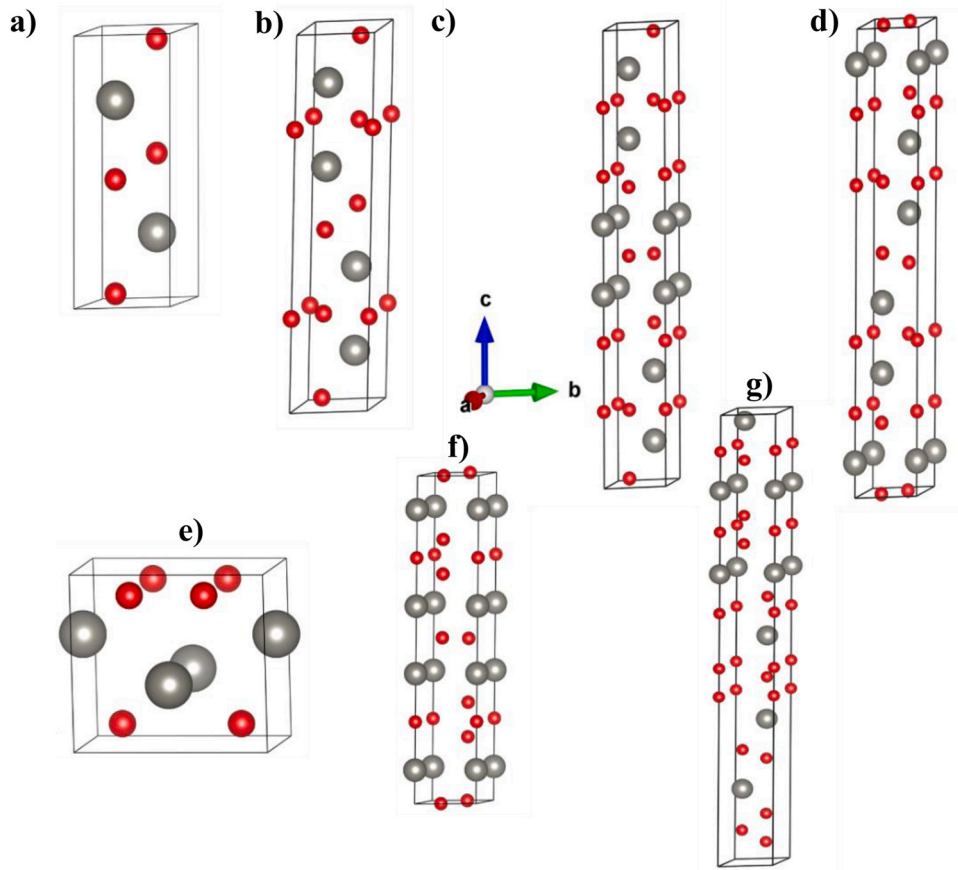


Fig. 3. Unit cell representations of the lowest-energy candidate structure of the ϵ phase: (a) WB_2 (hex^1) [30], (b) WB_2 (hex^2) [8], (c) WB_2 (Rm^1) [30], (d) WB_2 (Rm^2) [8], (e) WB_2 (O) [30], (f) W_2B_5 (hex) [30] and (g) W_2B_5 (tri) [57]. Grey/large atoms are W and red/small atoms are B. A superscript ¹ or ² indicate variations of the crystal with the same space group but different motif.

formation enthalpy structures at any composition range of interest. Thus, any compound whose formation enthalpy lies on the convex hull is thermodynamically stable and any that does not is deemed metastable [55,56], and the distance from the convex hull is representative of the energy gap to reach stability. Among the sixteen

structures investigated in the composition range of 67–71.4 at% B (WB_2 – W_2B_5), seven lower energy compounds were selected for further investigation, and their formation enthalpy was calculated also using the LDA exchange-correlation functional (Fig. 2b). Noting, four of these seven structures were proposed by Li et al. [30] through

Table 1

Crystal structure definition and formation enthalpies (per atom) of lowest-energy candidate structures of the ϵ phase. E_f reported from PBE calculations and, in square brackets, from LDA calculations.

Comp.	Space group	E_f (eV/atom)	Lattice Parameter (Å)	Wyckoff positions				Ref.			
				Atom	x	y	z				
WB ₂	hex ¹ (P6 ₃ /mmc)	-0.3632	a = 2.9269	W (2c)	0.333333	0.333333	0.666667	0.250000	[30]		
		[−0.3718]	c = 7.7507	B (4f)				0.540730			
	hex ² (P6 ₃ /mmc)	-0.3376	a = 2.9840	W1(4f)	0.333333	0.333333	0.666667	0.139000	[8]		
		[−0.3790]	c = 13.8700	B1 (4f)	0.333333		0.666667	-0.028000			
				B2(2d)	0.000000		0.666667	0.750000			
				B3(2b)			0.000000	0.250000			
	Rm ¹ (R-3 m)	-0.3435	a = 3.0135	W (6c)	0.000000		0.000000	0.576430	[30]		
		[−0.3841]	c = 21.0948	B1(6c)	0.000000		0.000000	0.681720			
				B2 (6c)	0.000000		0.000000	0.168050			
	Rm ² (R-3 m)	-0.3434	a = 3.0138	W (6c)	0.000000		0.000000	0.075100	[8]		
		[−0.3878]	c = 20.9541	B1(6c)	0.000000		0.000000	0.332900			
				B2(6c)	0.000000		0.000000	0.181000			
O (Pmmn)	-0.3575	a = 2.9187	W1(2b)	0.000000	0.500000	0.692610	0.379780	[30]			
	[−0.3776]	b = 4.6563 c = 4.2308	B1(4e)	0.000000			0.884460				
W ₂ B ₅	hex (P6 ₃ /mmc)	-0.2624	a = 3.0171	W1(4e) B1(2b)	0.000000	0.000000	0.000000	0.397090	0.250000	[30]	
		[−0.3038]	c = 15.7082	B2(4f) B3 (4f)	0.333333	0.333333	0.666667	0.666667	0.302580	0.497260	
	tri (R3m)	-0.2949	a = 2.9225	W1(3a)	0.666667	0.666667	0.333333	0.333333	0.981200	0.165900	[57]
		[−0.3197]	c = 5.9018	W2(3a)	0.666667	0.666667	0.333333	0.333333	0.074200	0.252500	
			B1 (3a)	0.333333		0.666667		0.042200			
			B2 (3a)	0.333333		0.666667		0.104900			
			B3 (3a)	0.333333		0.666667		0.227300			
			B4 (3a)								
			B5(3a)								

a global structural search using CALYPSO. These selected compounds are depicted in Fig. 3 and their crystal structures are described in Table 1. The results from the two levels of theory are in remarkable agreement, with only small changes that are within the expected level of precision of DFT, suggesting that the results are insensitive to the choice of exchange correlation function. Among these seven compounds, the compounds of WB₂ composition are closer to the convex hull than the compounds of W₂B₅ composition. None of the compounds of W₂B₅ composition (W₂B₅ (hex) and W₂B₅ (tri)) lies on the calculated convex hull, suggesting that this composition is metastable.

The ground-state calculations presented above were extended to include thermal effects by performing phonon simulations for the seven most promising structures and calculating the vibrational free energy within the harmonic approximation (Eq. 3). Fig. 4 shows the formation free energy of these structures at 300 K and 2500 K, obtained with the PBE and LDA exchange correlation functionals (via Eq. 2). A comparison between the formation enthalpy of these compounds at their ground state (Fig. 2) and higher temperatures indicates that inclusion of vibrational energy does not change the higher stability of WB₂ compounds compared to the W₂B₅ compounds. However, the order of stability of compounds within the WB₂ composition is somewhat affected by vibrational energy: at room temperature both WB₂ (hex¹) and WB₂ (Rm²) structures remain within DFT precision of the convex hull (as per the ground state), while at high temperature (2500 K), WB₂ (Rm²) appears to be metastable.

Fig. 5 shows temperature dependences of the formation free energy of different compounds of WB₂ and W₂B₅ compositions, obtained with the LDA and PBE functionals. The cross-over in stability occurs around 1300 K, however, for four compounds (W₂B₅ (hex), W₂B₅ (tri), WB₂ (hex¹) and WB₂ (O)) the range of formation energies remains within the bounds of uncertainty of DFT calculations. Note also that the harmonic approximation used here does not include the effect of thermal expansion, the presence of defects, and anharmonic effects, none of which are expected to play a significant role until elevated temperature, and unlikely to be significant at 300 K. Overall, no significant changes are observed in the

metastability of the compounds of W₂B₅ composition, as they lie above the convex hull at all temperatures.

3.2. Dynamical and mechanical stability

To investigate dynamic stabilities of structures considered, phonon calculations were carried out. It is well established that the PBE (LDA) exchange correlation functional produces higher (lower) values of lattice parameters than experimental values, and for some materials with significant mass difference in the constituent elements (e.g. PdH) [58] this can affect the phonon results drastically. For this reason, we repeat the calculations at both levels of theory. Fig. 6 shows the results of the phonon calculations with both PBE (solid blue) and LDA (dashed black) functionals. Both approximations lead to essentially identical results, except for a small shift to higher frequencies of LDA, as expected from the slightly reduced lattice parameters. Importantly, no soft modes are present in the phonon dispersion curves of all structures of interest, with both levels of theory, which is a strong sign of dynamic stability.

The elastic constants (c_{ij}) of the candidate structures are reported in Table 2. All structures satisfied the Born-Huang mechanical stability criteria [59–62]. All candidate structures exhibit stiff constants, in excess of 500 GPa for c_{11} , c_{22} and c_{33} . Notably, the WB₂ (hex¹) structure possesses a remarkably high value of c_{33} (\approx 950 GPa), indicating a stiffness along the c axis akin to diamond ($c_{ij}^{diamond} \approx$ 1000 GPa) [38,63]. For all structures, c_{11} and c_{44} are not equal to c_{33} and c_{66} , respectively, indicating elastic anisotropy [64].

The bulk modulus (B), shear modulus (G), Poisson's ratio (ν) [65], Pugh's modulus ratio (G_H/B_H) [66] and Cauchy pressure ($c_{12} - c_{44}$) [67,68] of polycrystalline aggregates here were calculated from the elastic constants, and are reported in Table 3. WB₂ (hex²) possesses the most incompressibility ($B \sim$ 350 GPa) and accordingly the strongest $W-d$ and $B-p$ orbital hybridization among all other candidates [69]. Conversely, WB₂ (hex¹) has the highest shear resistance, of about 275.2 GPa. For all candidates except WB₂ (O), the values of ν and Cauchy pressure are less than 0.26 and 0, respectively, which together with the positive value of G_H/B_H , indicate brittleness of

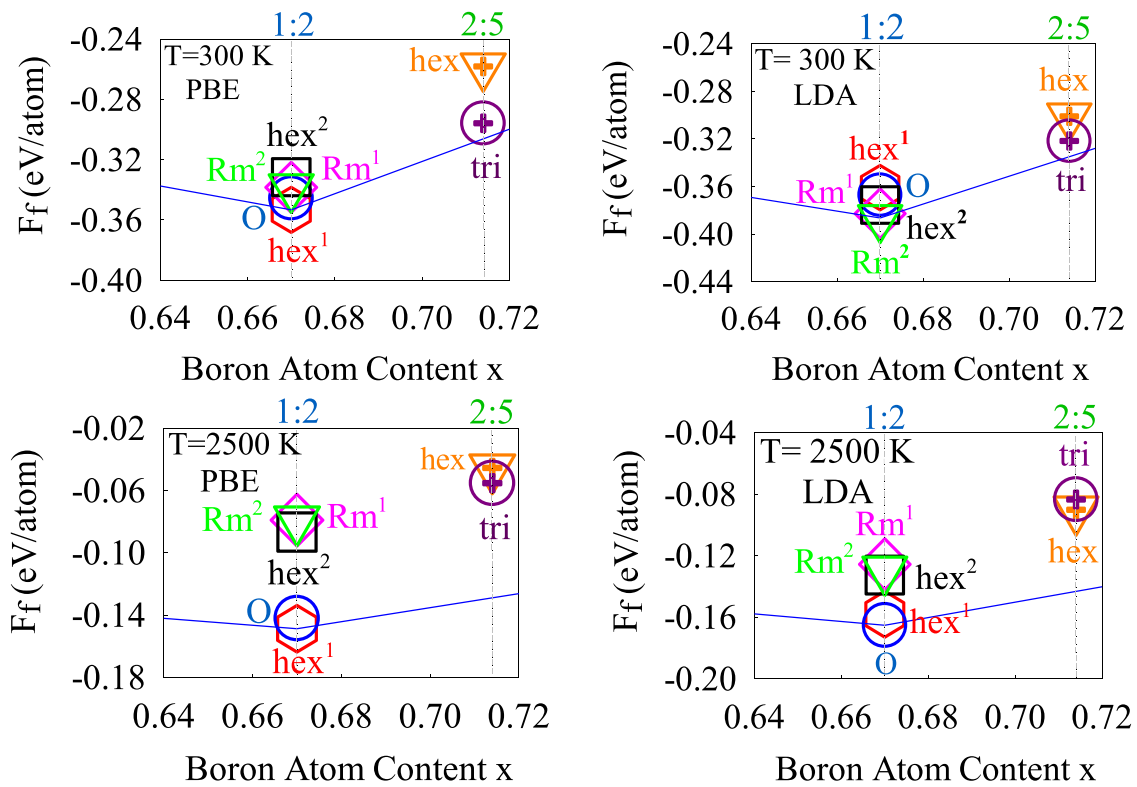


Fig. 4. Formation free energy of different compounds of WB_2 and W_2B_5 compositions, obtained with the PBE and the LDA exchange correlation functionals at different temperatures.

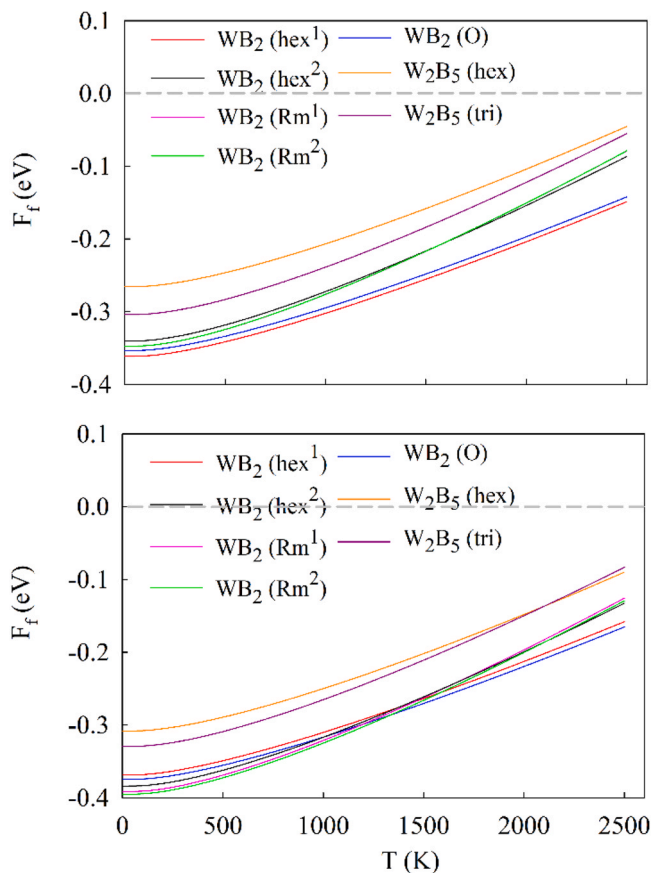


Fig. 5. Temperature dependences of the formation free energy of different compounds of WB_2 and W_2B_5 compositions, obtained with the PBE (upper panel) and LDA (lower panel) exchange correlation functionals.

these structures. Fig. 7 shows calculated bulk modulus (B), shear modulus (G) and Poisson's ratio (ν) of these candidates, graphically.

Cheng et al. [38] found a strong correlation between mechanical properties and thermodynamic stability of the W-B system, claiming the compound with the lowest formation energy for a given composition possesses the smallest Poisson's ratio and the largest shear modulus. Such strong correlations were also observed in our calculations.

In the next section we explore the ability of the proposed structures to accommodate deviations of stoichiometry through point defects.

3.3. Dilute point defect

Deviation of stoichiometry may be accommodated by interstitials, vacancies, and anti-site defects. Specifically, the presence of W vacancies and B interstitials leads to hyper-stoichiometry (boron-rich compositions) while B vacancies lead to hypo-stoichiometry (boron-poor compositions). W interstitial would also lead to hypo-stoichiometry, however these are very large defects that are likely to have large associated energy (as observed for in WC [70] and for uranium interstitials in the related compound UB_2 [71]). Similarly, anti-site defects (W on B site and vice-versa) are unlikely to be easily accommodated in tungsten borides. Fig. 8 shows the formation enthalpy of tungsten and boron interstitials, and tungsten vacancies for the structures considered in this study.

Negative vacancy formation energies are observed for four structures: WB_2 (hex^2), WB_2 (Rm^1), WB_2 (Rm^2) and W_2B_5 (hex). This implies that the defects would form spontaneously, and is clear sign of structural instability of the stoichiometric compound. The ability to accommodate large deviations of stoichiometry is usually manifest in a small but positive formation energy of the defect through which the deviation is accommodated. However, a negative defect formation could also indicate a strong drive toward non-

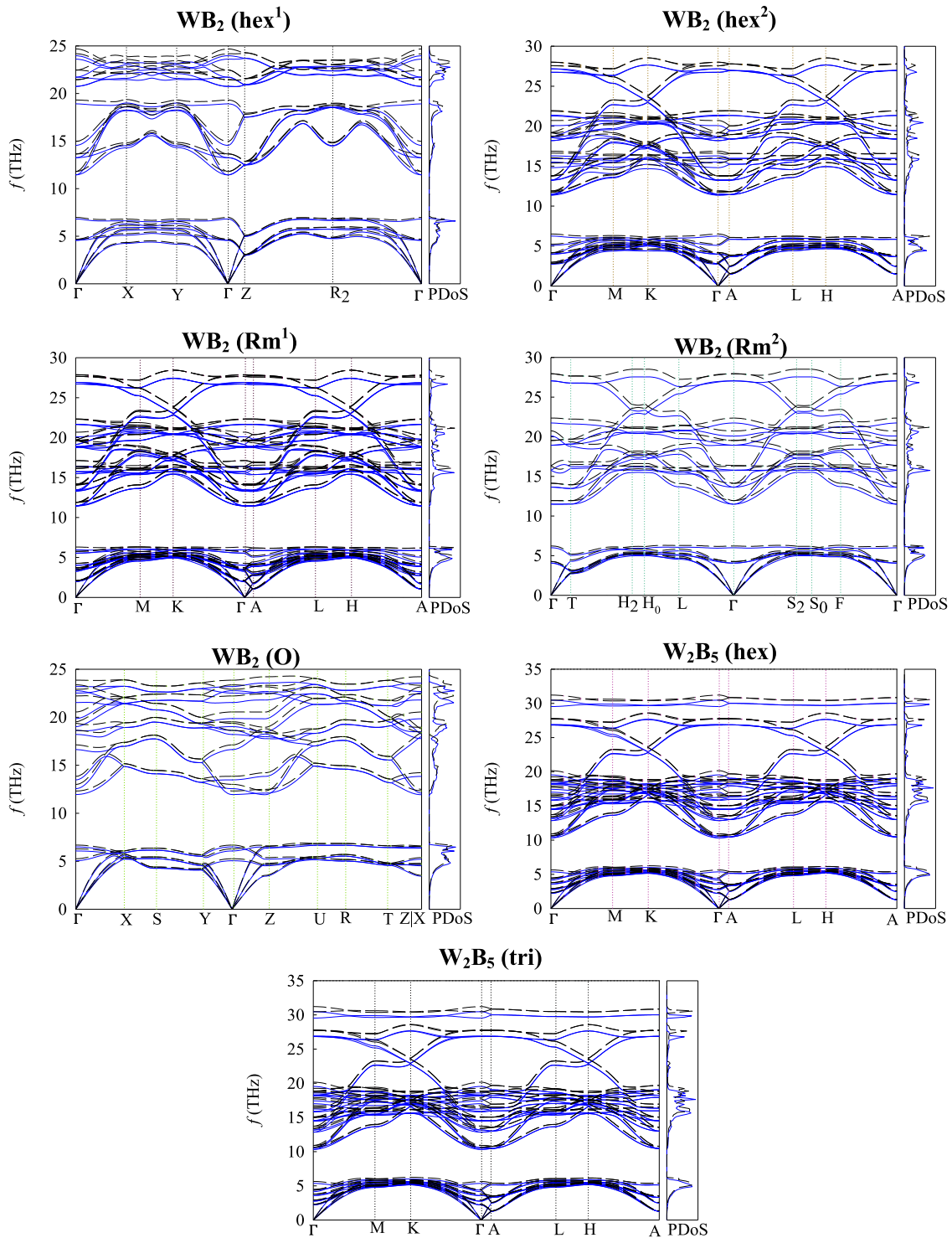


Fig. 6. Phonon band structure and density of state of candidate structures of the ϵ phase, obtained with the PBE (blue/solid lines) and LDA (black/dashed lines) exchange-correlation functionals.

stoichiometry, provided that the addition of further defects leads, eventually, to an increase in the defect formation energy above zero. The negative formation energy of defects for the WB_2 (hex^2) and WB_2 (Rm^1) structures is in good accordance with their formation enthalpies, which lie well above the free energy convex hulls (Fig. 2a), indicating their metastability. On the other hand, WB_2 (Rm^2) structure is found to be within DFT precision of the convex hull, and combining this with the negative formation of B2 vacancies, it would suggest that if the compound were stable it would

have to have a significantly reduced stoichiometry from that reported experimentally. Finally, for W_2B_5 (hex), while it has a free energy of formation significantly above the convex hull, this reduces significantly when a concentration of B vacancies is added to the structure, each with an associated formation energy of -0.578 eV, and concurrently reducing the stoichiometry closer to the more commonly reported values. Whether the reduction in energy through the introduction of vacancies is sufficient to stabilise the structure cannot be said without a further dedicated study.

Table 2
Calculated elastic constants c_{ij} (in GPa) for the seven leading candidate structures of the ϵ phase.

Structure	c_{11}	c_{22}	c_{33}	c_{12}	c_{13}	c_{23}	c_{44}	c_{55}	c_{66}
WB ₂ (hex ¹)	591.3	591.8	953.4	174.6	106.4	106.2	283.9	283.8	208.2
WB ₂ (hex ²)	612.8	612.8	726.3	149.9	26.44	186.2	230.6	230.6	231.4
WB ₂ (Rm ¹)	596.1	596.1	701.2	146.4	202.3	202.3	237.6	237.6	224.9
WB ₂ (Rm ²)	596.5	596.5	702.2	146.5	202.1	202.1	237.8	237.8	225.0
WB ₂ (O)	570.0	514.6	875.6	217.3	72.75	171.5	196.9	313.7	242.0
W ₂ B ₅ (hex)	559.2	559.2	698.2	159.2	200.1	200.1	212.6	212.6	200.0
W ₂ B ₅ (tri)	556.6	556.6	838.9	147.0	152.4	152.4	277.6	277.6	204.8

Table 3

Bulk modulus from Hill average (B_H) of Voigt (B_V) and Reuss (B_R) moduli, and same for Shear modulus, G , Poisson's ratio (ν), Pugh's modulus ratio (G_H/B_H), and Cauchy pressure $c_{12} - c_{44}$ of the leading candidate structures of the ϵ phase.

Structure	Bulk modulus (GPa)			Shear modulus (GPa)			ν	G_H/B_H	$c_{12} - c_{44}$
	B_H	B_V	B_R	G_H	G_V	G_R			
WB ₂ (hex ¹)	316.3	320.2	312.5	275.2	285.4	265.0	0.1628	0.8700	-109.3
WB ₂ (hex ²)	350.0	329.6	370.4	242.4	245.5	239.2	0.2187	0.6925	-80.7
WB ₂ (Rm ¹)	321.0	329.5	312.5	237.0	241.0	232.9	0.2038	0.7382	-91.2
WB ₂ (Rm ²)	331.5	329.6	333.3	236.4	241.2	231.5	0.2120	0.7130	-91.3
WB ₂ (O)	314.9	317.2	312.7	249.0	263.0	235.1	0.1871	0.7907	20.4
W ₂ B ₅ (hex)	313.0	322.9	303.0	218.0	224.2	211.9	0.2173	0.6966	-53.3
W ₂ B ₅ (tri)	295.9	314.1	277.8	256.7	264.6	248.8	0.1636	0.8674	-130.6

For five structures there are multiple distinct boron sites (denoted by a number in Fig. 8), each with a different vacancy formation energy. In the case of WB₂ (hex²), WB₂ (Rm¹), WB₂ (Rm²) and W₂B₅

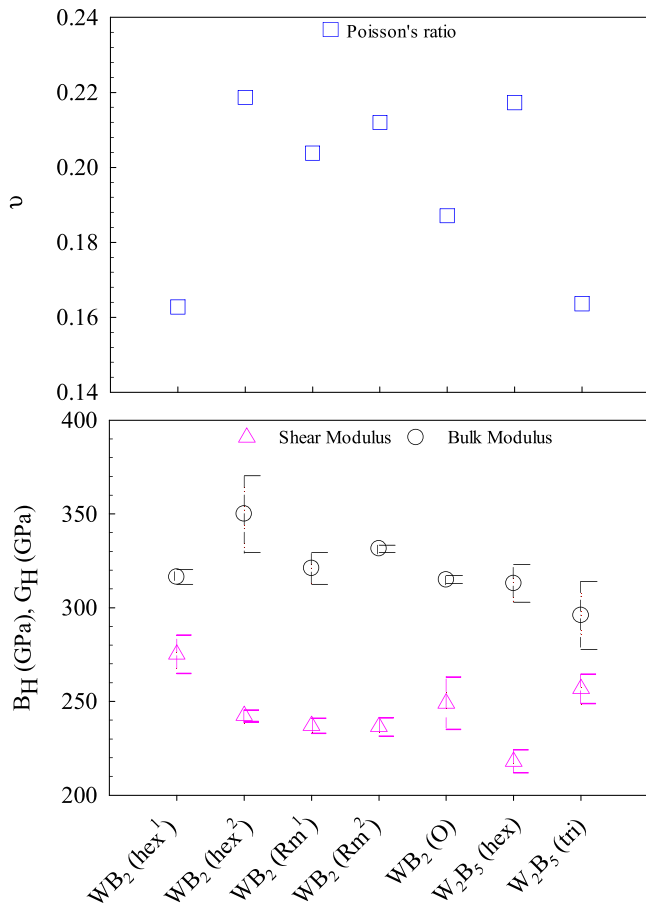


Fig. 7. Poisson's ratio (top panel), bulk and shear moduli (bottom panel) of the leading candidate structures of the ϵ phase. The error bars represent the range between Reuss and Voigt values and the symbols indicate the average (Hill value).

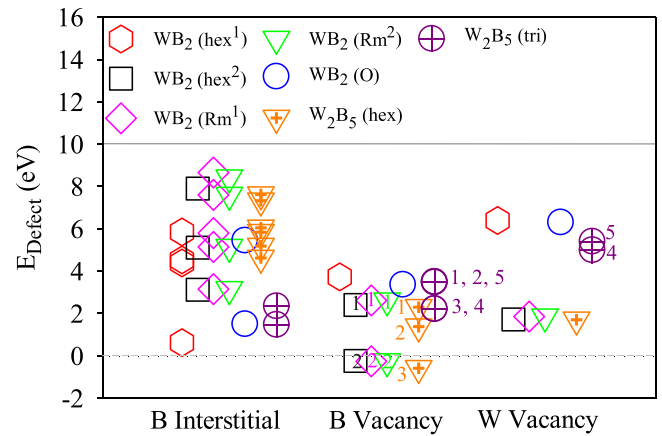


Fig. 8. Formation energies of point defects the leading candidate structures of the ϵ phase. Where multiple non-equivalent sites exist for vacancies, these are denoted by numbers (e.g. B1 of Table 1 denoted as 1).

(hex), one of these displays negative formation energy, while the others exhibit positive formation energy. For the W₂B₅ (tri) structure, five symmetrically distinct sites exhibit, however their formation energies fall on of two energy levels, due to similar local environments: vacancies on site 3 and 4 have $E_{\text{Defect}} = 2.2$ eV and those on site 1, 2 and 5 have $E_{\text{Defect}} = 3.5$ eV.

3.4. XRD and neutron diffraction simulations

Figs. 9 and 10 illustrate simulate x-ray ($\lambda = 1.5418$ Å) and neutron ($\lambda = 1.54816$ Å) diffraction patterns for the structures of interest, respectively, compared to available experimental data for the ϵ phase [28,33]. The experimental XRD and neutron patterns of the ϵ phase are best fit by WB₂ (hex²). However, this structure is metastable since it lies well above the convex hull and possesses negative formation enthalpy of point defects which is a clear sign of structural instability of the stoichiometric compound. This indicates that the true structure may perhaps be a variation of WB₂ hex², with a similar long-range order but different local environment, perhaps akin to

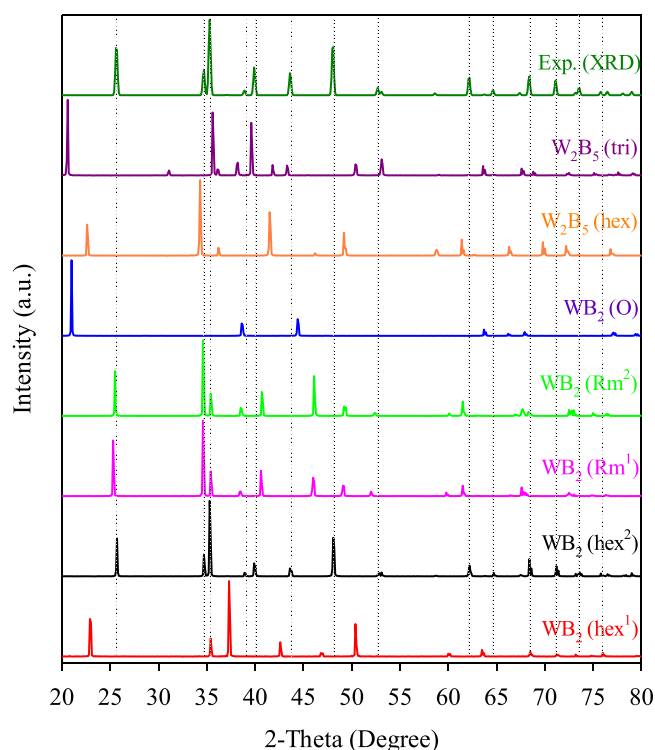


Fig. 9. Simulated XRD patterns of the leading candidate structure of the ϵ phase, including the experimental data of Kayhan et al. [28,33].

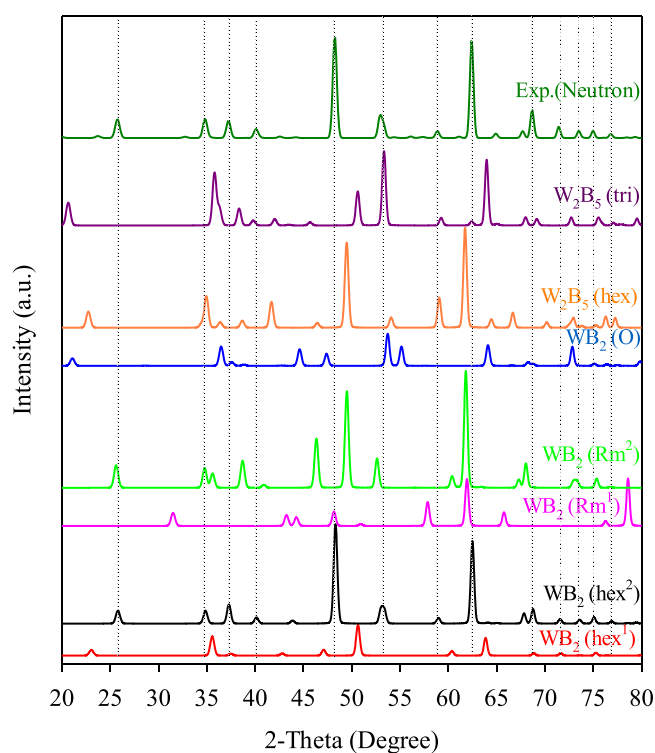


Fig. 10. Simulated neutron patterns of the leading candidate structures of the ϵ phase, including the experimental data of Kayhan et al. [28,33].

that of other candidate structure that lie on the convex hull. It must be stressed that one expects some degree of disagreement between DFT lattice parameter and experiment, typically within 5%, which

would move all reflection by varying degree. Even so, it can be stated with confidence that the reflections of the Pmmn space group are incompatible with the experimental ones, while the space groups R-3 m and P6₃/mmc both provide reasonable starting point for further refinement.

Neither of the metastable compounds of W₂B₅ (hex and tri) exhibit convincing diffraction patterns, in agreement with the DFT observation that this composition is metastable. However, since the free energy of W₂B₅ (hex) reduces significantly when a concentration of B vacancies is added to this structure, simultaneously reducing its stoichiometry, the true experimental structure might be a variation of this structure with a similar space group where either the boron sites occupancy or the stacking of layers is slightly different. To further advance our understanding of this structure, a new set of accurate neutron diffraction measurements of the ϵ phase, with B-11 enrichment, high chemical purity and high resolution, is required to confirm and refine the position and occupancy of the boron atoms for this structure.

4. Conclusions

DFT calculation were undertaken to revisit the literature and identify the structure and composition of the ϵ phase of tungsten boride. From a starting pool of 16 potential structures available in literature in the composition range of 67–71.4 at% B (WB₂–W₂B₅), seven were found to be promising candidates for this phase on the basis of a convex hull analysis of the free energy of formation, including vibrational thermal contributions. The seven candidates are: WB₂ (hex¹), WB₂ (hex²), WB₂ (Rm¹), WB₂ (Rm²), WB₂ (O), W₂B₅ (hex) and W₂B₅ (tri). Four of these seven structures were proposed via employing computational global structural search algorithms in previous studies.

All seven structures were found to be dynamically stable (no soft phonon modes) and mechanically stable (satisfied Born-Huang criteria). All candidates are predicted to be stiff (bulk moduli 300–350 GPa), brittle and display significant elastic anisotropy.

We considered the possibility that the ϵ phase may in fact be non-stoichiometric by calculating the point defect formation energy for all candidate structures. Four structures exhibited negative vacancy formation energy: WB₂ (hex²), WB₂ (Rm¹), WB₂ (Rm²) and W₂B₅ (hex). Since negative formation enthalpy of point defects is an obvious indication of structural instability, so these four structures are either unstable, or the true nature of these compounds is hypo-stoichiometric (boron-deficient). However, in the case of WB₂ compounds, this would take the overall composition far from experimental observation, while in the case of W₂B₅ (hex) it would bring it in closer agreement. Comparing simulated diffraction patterns of the candidate structures with experimental x-ray and neutron diffraction measurements, it is evident that the Pmmn space group is incompatible with experimental diffraction patterns, while P6₃/mmc, R-3 m and R3m are plausible.

By combining ab initio calculations with comparisons of X-ray and neutron diffraction data, we propose that the true experimental structure of the ϵ phase might be a non-stoichiometric W₂B_{5-x} composition with space group P6₃/mmc. The DFT results are in good agreement with the available XRD and neutron diffraction measurements. However, further work is required to verify the extent of hypo-stoichiometry in the ϵ phase of W₂B_{5-x}.

CRediT authorship contribution statement

S.S.S. performed the DFT simulations. All authors contributed to the manuscript, which was edited by **S.S.S** and **P.B.**

Declaration of Competing Interest

The authors declare the following financial interests/personal relationships which may be considered as potential competing interests: Samaneh S. Setayandeh, Edward G. Obbard, Jennifer H. Stansby, Dillon Frost and Patrick A. Burr report financial support was provided by Tokamak Energy Ltd.

Acknowledgements

SSS, PAB and EO would like to thank Tokamak Energy (UK) for providing financial support. This research was supported by an Australian Government Research Training Program (RTP) Scholarships. This work was undertaken with the assistance of resources and services from the National Computational Infrastructure (NCI), which is supported by the Australian Government; the Multimodal Australian Science Imaging and Visualisation Environment (MASSIVE); the Pawsey Supercomputing Centre, which is supported by the Australian Government and the Government of Western Australia; and was enabled by Intersect Australia Limited. Learn more at www.intersect.org.au.

References

- N. Gonzalez Szwacki, The structure and hardness of the highest boride of tungsten, a borophene-based compound, *Sci. Rep.* 7 (1) (2017) 4082.
- S. Yazici, B. Derin, Double SHS of W₂B₅ Powder from CaWO₄ and B₂O₃, *Adv. Sci. Technol.* (2010).
- V.F. Funke, S.I. Yudovskii, G.V. Samsonov, *Hard alloys*, Metallurgizdat 92 (1962) 4.
- V.I. Matkovich, *Boron and Refractory Borides*, Springer-Verlag, New York, 1977.
- E. Zhao, X. Yuan, W. Zhang, Thermodynamic identification of tungsten borides from first principles calculations, *Phys. Chem. Chem. Phys.* 12 (40) (2010) 13158–13165.
- R.F. Zhang, et al., Stability and strength of transition-metal tetraborides and triborides, *Phys. Rev. Lett.* 108 (25) (2012) 255502.
- H. Gou, et al., Peculiar structure and tensile strength of WB₄:nonstoichiometric origin, *AIP Adv.* 2 (1) (2012) 012171.
- M. Frotscher, et al., M₂B₅ or M₂B₄? A reinvestigation of the Mo₂B and W₂B system, *Z. für Anorg. Allg. Chem.* 633 (15) (2007) 2626–2630.
- Y. Liang, X. Yuan, W. Zhang, Thermodynamic identification of tungsten borides, *Phys. Rev. B* 83 (22) (2011) 220102.
- X.-Q. Chen, et al., Electronic and structural origin of ultrahigh compressibility of 5d transition-metal diborides MB₂ (M=W, Re, Os), *Phys. Rev. Lett.* 100 (19) (2008) 196403.
- S.A. Gromilov, et al., Investigation of W₂B and β -WB high-temperature phases in coatings produced by a shaped charge explosion, *J. Struct. Chem.* 51 (6) (2010) 1126–1131.
- J. Yang, H. Sun, C. Chen, Is osmium diboride an ultra-hard material? *J. Am. Chem. Soc.* 130 (23) (2008) 7200–7201.
- M. STUBICAR, A. TONEJC, N. STUBICAR, X-ray diffraction study of W–B elemental powder mixtures after high-energy ball-milling, *Fiz. A* 4 (1) (1995) 65–72.
- K.A. Khor, L.G. Yu, G. Sundararajan, Formation of hard tungsten boride layer by spark plasma sintering boriding, *Thin Solid Films* 478 (1) (2005) 232–237.
- H. Kawanowa, et al., Structure analysis of the WB₂(0001) surface, *Surf. Sci.* 433–435 (1999) 661–665.
- M. Usta, et al., The characterization of borided pure tungsten, *Surf. Coat. Technol.* 194 (2) (2005) 330–334.
- K.-f. Cai, C.-W. Nan, The influence of W₂B₅ addition on microstructure and thermoelectric properties of B₄C ceramic, *Ceram. Int.* 26 (5) (2000) 523–527.
- S. Stadler, et al., Electronic structures of the tungsten borides WB, W₂B and W₂B₅, *J. Electron Spectrosc. Relat. Phenom.* 110–111 (2000) 75–86.
- S.A. Humphry-Baker, G.D.W. Smith, Shielding materials in the compact spherical tokamak, *Philos. Trans. R. Soc. A* 377 (2141) (2019) 20170443.
- C.G. Windsor, et al., Design of cemented tungsten carbide and boride-containing shields for a fusion power plant, *Nucl. Fusion* 58 (7) (2018) 076014.
- A. Sykes, et al., Compact fusion energy based on the spherical tokamak, *Nucl. Fusion* 58 (1) (2017) 016039.
- C.G. Windsor, et al., Tungsten boride shields in a spherical tokamak, *Nucl. Fusion* 61 (2021) 086018.
- R. Kieffer, F. Benesovsky, In *Hartstoffe*. Springer-Verlag, Vienna, 1963.
- R. Kieffer, The crystal structures of molybdenum and tungsten borides, *Acta Chem. Scand.* (1947) 1.
- H. Itoh, et al., Formation process of tungsten borides by solid state reaction between tungsten and amorphous boron, *J. Mater. Sci.* 22 (8) (1987) 2811–2815.
- S. Okada, K. Kudou, T. Lundström, Preparations and some properties of W₂B, δ -WB and WB₂ crystals from high-temperature metal solutions, *Jpn. J. Appl. Phys.* 34 (Part 1, No. 1) (1995) 226–231.
- H.P. Woods, J.F.E. Wagner, B.G. Fox, Tungsten diboride, preparation and structure, *Science* (1966) 151.
- M. Kayhan, et al., Neutron diffraction and observation of superconductivity for tungsten borides, WB and W₂B₄, *Solid State Sci.* 14 (11) (2012) 1656–1659.
- R. Mohammadi, et al., Tungsten tetraboride, an inexpensive superhard material, *PNAS* 108 (27) (2011) 10958–10962.
- Q. Li, et al., Global structural optimization of tungsten borides, *Phys. Rev. Lett.* 110 (13) (2013) 136403.
- T. Lundström, The structure of Ru₂B₃ and WB₂. 0 as determined by single-crystal diffraction, and some notes on the WB system, *Ark. Kemi* 30 (1969) 115–127.
- P.A. Romans, M.P. Krug, Composition and crystallographic data for the highest boride of tungsten, *Acta Cryst.* 20 (1966) 313–315.
- M. Kayhan, Transition metal borides Synthesis, characterization and superconducting properties, *Condens. Matter Phys. Superconduct. Superfluid.* (2013).
- C.W. Glass, A.R. Oganov, N. Hansen, USPEX—evolutionary crystal structure prediction, *Comput. Phys. Commun.* 175 (11) (2006) 713–720.
- A.R. Oganov, C.W. Glass, *Crystal structure prediction using ab initio evolutionary techniques: principles and applications*, *J. Chem. Phys.* 124 (24) (2006) 244704.
- A.O. Lyakhov, A.R. Oganov, M. Valle, How to predict very large and complex crystal structures, *Comput. Phys. Commun.* 181 (9) (2010) 1623–1632.
- C.J. Pickard, R.J. Needs, Ab initio random structure searching, *J. Phys. Condens. Matter* 23 (5) (2011) 053201.
- X.Y. Cheng, et al., Computational materials discovery: the case of the W–B system, *Acta Crystallogr. C Struct. Chem.* 70 (Pt 2) (2014) 85–103.
- G. Kresse, J. Hafner, Ab initio molecular dynamics for liquid metals, *Phys. Rev. B* 47 (1) (1993) 558–561.
- G. Kresse, J. Hafner, Ab initio molecular-dynamics simulation of the liquid-metal–amorphous-semiconductor transition in germanium, *Phys. Rev. B* 49 (20) (1994) 14251–14269.
- G. Kresse, J. Furthmüller, Efficiency of ab-initio total energy calculations for metals and semiconductors using a plane-wave basis set, *Comput. Mater. Sci.* 6 (1) (1996) 15–50.
- J.P. Perdew, A. Zunger, Self-interaction correction to density-functional approximations for many-electron systems, *Phys. Rev. B* 23 (10) (1981) 5048–5079.
- J.P. Perdew, K. Burke, M. Ernzerhof, Generalized gradient approximation made simple, *Phys. Rev. Lett.* 77 (18) (1996) 3865–3868.
- P.E. Blöchl, Projector augmented-wave method, *Phys. Rev. B* 50 (24) (1994) 17953–17979.
- G. Kresse, D. Joubert, From ultrasoft pseudopotentials to the projector augmented-wave method, *Phys. Rev. B* 59 (3) (1999) 1758–1775.
- H.J. Monkhorst, J.D. Pack, Special points for Brillouin-zone integrations, *Phys. Rev. B* 13 (12) (1976) 5188–5192.
- M. Methfessel, A.T. Paxton, High-precision sampling for Brillouin-zone integration in metals, *Phys. Rev. B* 40 (6) (1989) 3616–3621.
- B. Fultz, Vibrational thermodynamics of materials, *Prog. Mater. Sci.* 55 (4) (2010) 247–352.
- P. Giannozzi, et al., Ab initio calculation of phonon dispersions in semiconductors, *Phys. Rev. B* 43 (9) (1991) 7231–7242.
- A. Togo, I. Tanaka, First principles phonon calculations in materials science, *Scr. Mater.* 108 (2015) 1–5.
- R. Hill, The elastic behaviour of a crystalline aggregate, *Proc. Phys. Soc. Sect. A* 65 (5) (1952) 349–354.
- W. Voigt, *Lehrbuch der Kristallphysik*, Teubner Verlag, Leipzig, 1928.
- A. Reuss, Berechnung der fließgrenze von mischkristallen auf grund der plastizitätsbedingung für einkristalle, *ZAMM* 9 (1) (1929) 49–58.
- B.H. Toby, R.B. Von Dreele, GSAS-II: the genesis of a modern open-source all purpose crystallography software package, *J. Appl. Crystallogr.* 2 (46) (2013) 544–549.
- G. Ghosh, A. van de Walle, M. Asta, First-principles calculations of the structural and thermodynamic properties of bcc, fcc and hcp solid solutions in the Al–TM (TM=Ti, Zr and Hf) systems: A comparison of cluster expansion and supercell methods, *Acta Mater.* 56 (13) (2008) 3202–3221.
- X. Zhang, G. Trimarchi, A. Zunger, Possible pitfalls in theoretical determination of ground-state crystal structures: the case of platinum nitride, *Phys. Rev. B* 79 (9) (2009) 092102.
- C. Zhao, et al., Unexpected stable phases of tungsten borides, *Phys. Chem. Chem. Phys.* 20 (38) (2018) 24665–24670.
- S.S. Setayandeh, et al., Effect of pseudopotential choice on the calculated electron and phonon band structures of palladium hydride and its vacancy defect phases, *Int. J. Hydrog. Energy* 46 (1) (2021) 943–954.
- G.A. Alers, J. Neighbours R., Crystal stability and elastic constants, *AIP J. Appl. Phys.* 28 (12) (1957) 1514–1514.
- F. Mouhat, F.-X. Coudert, Necessary and sufficient elastic stability conditions in various crystal systems, *Phys. Rev. B* 90 (22) (2014) 224104.
- M. Born, K. Huang, In *Dynamical Theory of Crystal Lattices*, Clarendon Press, Oxford, 1954.
- Q.-J. Liu, et al., First-principles calculations of structural, elastic, and electronic properties of trigonal ZnSnO₃ under pressure, *Mater. Chem. Phys.* 180 (2016) 75–81.
- H.J. McSkimin, P. Andreatch, Elastic moduli of diamond as a function of pressure and temperature, *J. Appl. Phys.* 43 (7) (1972) 2944–2948.
- P. Li, et al., Elastic anisotropies and thermal conductivities of WB₂ diborides in different crystal structures: a first-principles calculation, *J. Alloy. Compd.* 747 (2018) 905–915.
- J.F. Nye, In *Physical Properties of Crystals*, Oxford University Press, 1979.

- [66] S.F. Pugh, XCII. Relations between the elastic moduli and the plastic properties of polycrystalline pure metals, Lond. Edinb. Dublin Philos. Mag. J. Sci. 45 (367) (1954) 823–843.
- [67] D.G. Pettifor, Theoretical predictions of structure and related properties of intermetallics, Mater. Sci. Technol. 8 (4) (1992) 345–349.
- [68] B. Huang, et al., Electronic structures, mechanical and thermodynamic properties of cubic alkaline-earth hexaborides from first principles calculations, J. Alloy. Compd. 635 (2015) 213–224.
- [69] S.V. Meschel, O.J. Kleppa, Standard enthalpies of formation of NbB₂, MoB, and ReB₂ by high-temperature direct synthesis calorimetry, Metall. Mater. Trans. A 24 (1993) 947.
- [70] P.A. Burr, S.X. Oliver, Formation and migration of point defects in tungsten carbide: Unveiling the sluggish bulk self-diffusivity of WC, J. Eur. Ceram. Soc. 39 (2) (2019) 165–172.
- [71] M. Iwasawa, et al., First-principles calculation of point defects in uranium dioxide. materials transactions, Mater. Trans. 47 (2006) 2651–2657.